

# Theory of Little–Parks oscillations by vortices in two-dimensional superconductors

Ying-Ming Xie<sup>1,\*</sup> and Naoto Nagaosa<sup>1, 2, †</sup>

<sup>1</sup>RIKEN Center for Emergent Matter Science (CEMS), Wako, Saitama 351-0198, Japan

<sup>2</sup>Fundamental Quantum Science Program (FQSP),  
TRIP Headquarters, RIKEN, Wako 351-0198, Japan

(Dated: February 2, 2026)

The Little–Parks (LP) effect is a quantum phenomenon in which the superconducting transition temperature of a superconducting cylinder (or ring) oscillates periodically as a function of the magnetic flux threading the loop. Recently, multiple experiments have observed half-quantum flux shifts in measurements of LP oscillations, where the oscillations are globally shifted by half a flux quantum compared to conventional cases, a behavior referred to as a  $\pi$ -ring. Such observations are commonly linked to unconventional pairing symmetries. In this work, we demonstrate that half-quantum flux shifts can arise in two-dimensional (2D) superconducting rings without invoking unconventional pairing symmetry, provided that vortices near the Berezinskii–Kosterlitz–Thouless (BKT) transition are taken into account. Specifically, based on the vortex-charge duality theory near the BKT transition, we map the problem onto a Coulomb gas model, in which the magnetic flux is represented as a pair of opposite boundary charges (or vortices) at the two edges. The screening of these boundary charges by thermally excited vortex-antivortex pairs is investigated through explicit Monte Carlo simulations. Importantly, we demonstrate that the oscillation of the free-vortex density as a function of magnetic flux can exhibit an anomalous half-quantum flux shift, depending on the geometry of the sample. Our work thus predicts the LP oscillations induced by vortices in 2D superconducting rings near the BKT transition, which provides a new mechanism for generating  $\pi$ -rings.

*Introduction.*— Superconducting quantum phenomena play important roles in quantum computation and quantum information processing. One of the earliest experiments demonstrating the quantum nature of superconductors is the observation of quantized magnetic flux trapped in units of the flux quantum  $\Phi_0 = h/(2e)$  in a multiply connected superconductor [1, 2], where  $h$  is Planck’s constant and  $e$  is the elementary charge. Following these experiments, Little and Parks studied thin-walled superconducting cylinders subjected to a magnetic field flux and showed that the resistance oscillates with a period of  $\Phi_0$ , due to the periodic change in superconducting transition temperature  $T_c$  [3, 4]. This Little–Parks (LP) effect can be understood within Ginzburg–Landau theory [5, 6], in which the magnetic field enters as a gauge potential, analogous to the Aharonov–Bohm effect.

The LP effect has also been used as a probe of unconventional superconductivity. Following the discovery of high-temperature superconductors and heavy-fermion superconductors, a half-quantum flux shift, or equivalently a  $\pi$ -phase shift, in a superconducting ring was proposed as a diagnostic of spin-triplet pairing or other unconventional pairing symmetries [7–9]. Especially, chiral spin-triplet pairing can generate an intrinsic and topologically protected phase winding in the superconducting condensate [10, 11], which can lead to a  $\pi$ -phase shift in the LP effect analogous to the half-quantum vortices observed in the  $^3\text{He}-\text{A}$  phase [12]. Recently, multiple experiments have reported  $\pi$ -phase shifts or half-quantum flux

states in superconducting rings without junction regions, including  $\beta$ -Bi<sub>2</sub>Pd [13],  $\alpha$ -BiPd [14], TaS<sub>2</sub> [15, 16], Bi/Ni bilayers [17], CsV<sub>3</sub>Sb<sub>5</sub> [18], and 2M-WS<sub>2</sub> [19]. Notably, these experiments commonly suggest that the emergence of half-quantum flux shift is associated with the possible presence of chiral or spin-triplet superconducting pairing. These experimental advances have also stimulated renewed theoretical interest in this phenomenon [20–23].

However, an important aspect has so far been overlooked. These recent experiments are typically performed on thin flakes, probably corresponding to the two-dimensional (2D) limit, and the resistance oscillations are measured at temperatures near the onset of finite resistance, which is usually close to the BKT transition temperature  $T_{\text{BKT}}$ . This raises a crucial question: how does the LP effect behave in the presence of vortices near the BKT transition in 2D superconductors? In particular, can the anomalous half-quantum flux shift be driven by BKT physics without involving unconventional pairing?

In this work, we present a systematic study of the LP effect in a conventional 2D superconducting cylinder or ring near the BKT transition (the geometry is schematically illustrated in Fig. 1(a) and (b)). We first construct a vortex-charge duality theory and map the problem onto a 2D neutral Coulomb gas model, in which the magnetic flux is mapped to boundary charges [Fig. 1(c)]. The bulk charges tend to screen these boundary charges in order to reduce the effective electric field in the bulk. We explicitly perform Monte Carlo simulations to investigate the effects of the boundary charges. Near the BKT transition, resistance oscillations are expected to be proportional to the density of free vortices. As the magnetic flux modifies the boundary charges with a period of  $\Phi_0$ ,

\* yingming.xie@riken.jp

† nagaosa@riken.jp

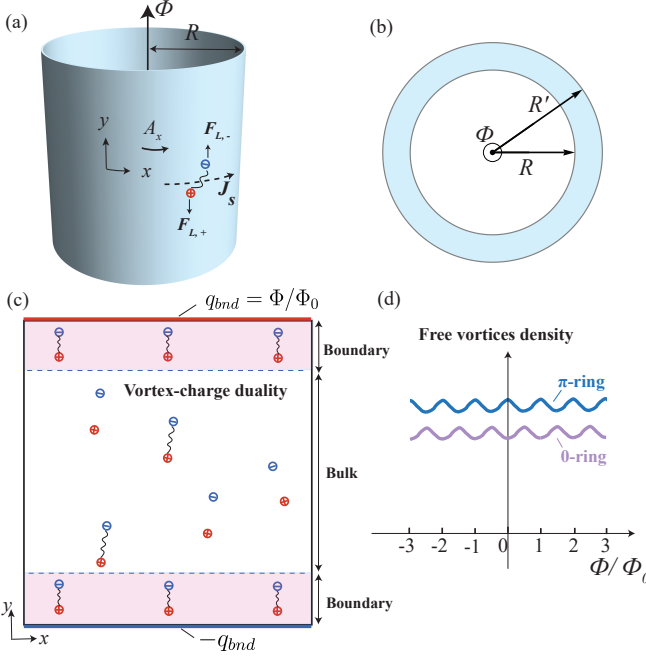


FIG. 1. (a,b) Schematic illustrations of a hollow superconducting cylinder and a ring, where the wall thickness is in the 2D limit. A magnetic flux  $\Phi$  threads the central hole of the cylinder or ring, with radii labeled  $R$  and  $R'$ , respectively. The  $\mathbf{F}_{L,\pm}$  labels the Lorentz forces. (c) Representation of the cylinder in panel (a) after the vortex-charge duality mapping, where the  $x$  direction is periodic and the  $y$  direction is open. The total boundary charge  $q_{bnd} = \pm\Phi/\Phi_0$  uniformly spreads at top and bottom, respectively (red and blue indicate opposite charges). Note that a shift by  $n\Phi_0$  can be absorbed into the phase winding around the hole of the cylinder. Charge pairs represent vortex-antivortex pairs, with bound pairs indicated by those connected by a curved line. Near the boundaries (pink), vortex charges tend to form aligned dipoles that screen the boundary charges. (d) Free-vortex density as a function of magnetic flux at 0- and  $\pi$ -ring cases.

we find that the free-vortex density exhibits periodic oscillations, leading to the LP behavior in practice. Importantly, we demonstrate how the half-quantum flux shift can appear in 2D superconducting cylinder/rings over a wide parameter regime through field-modified vortex dynamics near the BKT transition [see illustrations in Fig. 1(c) and (d)]. In this mechanism, the boundary charges act as effective pinning sources that reduce the density of free vortices, resulting in resistance peaks at integer flux. Our theory therefore establishes a BKT mechanism for half-quantum flux shift in superconducting rings and advances the understanding of the LP effect in 2D superconductors.

*Duality theory for 2D superconductors near the BKT transition.*— For completeness, we begin by presenting the field theory near the BKT transition in the presence of external gauge fields. The partition function is given

by  $Z = \int D[\theta(r, \tau)] \exp[-S]$ , and the action  $S$  is [24]

$$S = \int_0^\beta d\tau \int d^2\mathbf{r} \frac{J}{2} [(\partial_\tau \theta)^2 + (\nabla \theta)^2]. \quad (1)$$

Here  $\tau$  is the imaginary time,  $\beta = 1/(k_B T)$ ,  $\mathbf{r} = (x, y)$ , and  $J$  is the phase stiffness. The action arises from phase fluctuations of the superconducting order parameter,

$$\Delta(\mathbf{r}, \tau) = |\Delta(\mathbf{r}, \tau)| e^{i\theta(\mathbf{r}, \tau)} = \Delta_0 e^{i\theta(\mathbf{r}, \tau)}. \quad (2)$$

The phase field  $\theta(\tilde{x})$ , with  $\tilde{x} = (\mathbf{r}, \tau)$ , can be separated into a smooth part  $\theta_0(\tilde{x})$  and a singular vortex contribution  $\theta_v(\tilde{x})$  [24],

$$\theta(\tilde{x}) = \theta_0(\tilde{x}) + \theta_v(\tilde{x}). \quad (3)$$

For example, for a vortex core located at  $\mathbf{X} = (X_1, X_2)$ , the singular part is  $\theta_v(\mathbf{r}) = \arctan[(r_2 - X_2)/(r_1 - X_1)]$ . The vortex current is given by  $j_\mu = \frac{1}{2\pi} \epsilon_{\mu\nu\lambda} \partial_\nu \partial_\lambda \theta_v(\tilde{x})$ , which satisfies  $(\partial_1 \partial_2 - \partial_2 \partial_1) \theta_v(\mathbf{r}) = 2\pi \delta(\mathbf{r} - \mathbf{X}(\tau))$  [24]. Here the indices  $\mu, \nu, \lambda = 0, 1, 2$  label  $(\tau, x, y)$ . In particular,  $j_0(\mathbf{r}, \tau) = \delta(\mathbf{r} - \mathbf{X}(\tau))$  gives the vortex density, while  $j_\alpha(\mathbf{r}, \tau) = \partial_\tau X_\alpha(\tau) \delta(\mathbf{r} - \mathbf{X}(\tau))$  describes the spatial vortex current.

Next, we introduce the gauge potential into the action and establish the dual theory via a Hubbard-Stratonovich (HS) transformation. Specifically, the action becomes

$$S = \int d^3\tilde{x} \frac{J}{2} (\partial_\mu \theta + 2eA_\mu)^2, \quad (4)$$

where  $A_\mu$  denotes the gauge potential. After the HS transformation, the partition function takes the form  $Z = \int D\theta_0 D\theta_v DJ_\mu \exp[-\tilde{S}]$ , with

$$\tilde{S} = \int d^3\tilde{x} \left( \frac{J_\mu^2}{2J} + iJ_\mu [\partial_\mu \theta_0 + \partial_\mu \theta_v + 2eA_\mu] \right). \quad (5)$$

Integrating out  $\theta_0$  imposes the conservation law  $\partial_\mu J_\mu = 0$ , which can be solved as  $J_\mu = \frac{1}{2\pi} \epsilon_{\mu\nu\lambda} \partial_\nu a_\lambda$ . For compactness, we denote  $J_{3D} = \frac{1}{2\pi} \nabla_{3D} \times a_{3D}$ . It is straightforward to show that  $\int d^3\tilde{x} J_\mu \partial_\mu \theta_v = \int d^3\tilde{x} a_\lambda j_\lambda$  and  $2e \int d^3\tilde{x} J_\mu A_\mu = \frac{e}{\pi} \int d^3\tilde{x} a_\lambda B_\lambda$ . The resulting total action is

$$\begin{aligned} \tilde{S}' = \mathcal{A} \sum_i \int ds_i + \int d^3\tilde{x} & \frac{(\nabla_{3D} \times a_{3D})^2}{8\pi^2 J} \\ & + i \int d^3\tilde{x} a_{3D} \cdot (j_{3D} + \frac{e}{\pi} B_{3D}). \end{aligned} \quad (6)$$

The first term on the right-hand side represents the energy cost of vortex cores, with action  $\mathcal{A}$  per unit length multiplied by the length of the world line  $\int ds_i$  of the  $i$ th vortex. In the static 2D limit,  $a_{3D} \mapsto a_0(\mathbf{r})$ ,  $j_\mu \mapsto j_0 = \rho_v(\mathbf{r})$ , and  $B_{3D} \mapsto B_0 = B_z$ , yielding

$$\tilde{S}' = \beta \int d^2\mathbf{r} \{ \mathcal{A} |\rho_v(\mathbf{r})| + ia_0(\mathbf{r})(\rho_v(\mathbf{r}) + \frac{e}{\pi} B_z) + \frac{|\nabla a_0(\mathbf{r})|^2}{8\pi^2 J} \}. \quad (7)$$

The action  $\tilde{S}'$  describes a 2D neutral Coulomb gas, where  $\rho_v(\mathbf{r})$  denotes the vortex charge density. As an illustration, we set  $B_z = 0$  and write the vortex density as  $\rho_v = \sum_i q_i \delta(\mathbf{r} - \mathbf{X}_i)$ , where  $i$  labels the  $i$ th vortex and  $q_i = \pm 1$  corresponds to a vortex or antivortex. By integrating out the scalar field, an effective action is obtained [see Supplementary Material (SM) [25]]

$$\tilde{S}_{eff} = \frac{1}{2} \sum_{i \neq j} q_i q_j V(\mathbf{X}_{ij}) + E_c \sum_i q_i^2, \quad (8)$$

where  $\mathbf{X}_{ij} = \mathbf{X}_i - \mathbf{X}_j$ ,  $E_c$  is the vortex core energy, and the interaction takes the 2D logarithmic Coulomb form  $V(\mathbf{X}_{ij}) = -2\pi J \ln \frac{|\mathbf{X}_{ij}|}{r_c}$ , with  $r_c$  a short-distance cut-off. Defining the charge unit as  $\sqrt{2\pi J}$ ,  $\tilde{S}_{eff}$  is explicitly identified as a 2D neutral Coulomb gas model.

*Dual-field theory description of the LP effect for 2D superconductors.*— In the LP effect, a superconductor forms a ring of radius  $R$  threaded by a magnetic flux  $\Phi$ . As shown in Fig. 1(a), we consider a 2D superconductor with cylindrical topology, where the  $x$  direction is periodic and the  $y$  direction is open. Inside the sample,  $B_z = 0$ , while the vector potential  $\mathbf{A} = \frac{\Phi}{2\pi R} \hat{e}_x$  remains finite, analogous to the Aharonov–Bohm effect. A narrow 2D ring ( $|R' - R|/R \ll 1$ ), illustrated in Fig. 1(b), is geometrically equivalent to the system in Fig. 1(a). This equivalence is obtained by replacing the system length along the  $y$  direction,  $L_y$ , in Fig. 1(a) with the ring width  $|R' - R|$  in Fig. 1(b). The central question is how such a vector potential modifies the duality theory and whether it leads to novel physical consequences for the LP effect in 2D superconductors near the BKT transition.

Next, we show that the vector potential in the ring or cylinder geometry of 2D superconductors induces boundary vortex charges in the dual theory. Specifically, starting from the dual action, the coupling to the external field in the case of  $\nabla_{3D} \times A_{3D} = 0$  can be reduced to a boundary term,

$$\frac{ie}{\pi} \int d^3 \tilde{x} (\nabla_{3D} \times a_{3D}) \cdot A_{3D} = \frac{ie\beta}{\pi} \int_{\partial V} d^2 \mathbf{r} \cdot (a_{3D} \times A_{3D}), \quad (9)$$

where we have used the vector identity  $\text{div}(a_{3D} \times A_{3D}) = A_{3D} \cdot (\nabla_{3D} \times a_{3D}) - a_{3D} \cdot (\nabla_{3D} \times A_{3D})$ . The vector product is given by  $a_{3D} \times A_{3D} = (a_x A_y - a_y A_x, a_y A_0 - a_0 A_y, a_0 A_x - a_x A_0)$ . In the cylindrical geometry,  $A_0 = 0$  and  $(A_x, A_y) = (\frac{\Phi}{2\pi R}, 0)$ . We find that the right-hand side of Eq. (9) reduces to a boundary term  $i\beta \int d^2 \mathbf{r} \rho_v^{(A)} a_0(\mathbf{r})$ , with the boundary charge

$$\rho_v^{(A)}(\mathbf{r}) = \frac{q_{bnd}}{L_x} [\delta(y - L_y) - \delta(y)]. \quad (10)$$

Here, the boundary charge  $q_{bnd} = \frac{\Phi}{\Phi_0}$ ,  $\Phi_0 = \frac{\pi}{e}$  is the superconducting flux quantum (with  $\hbar = 1$ ), and the cylinder perimeter is  $L_x = 2\pi R$ . The term  $\rho_v^{(A)}(\mathbf{r})$  represents boundary charges  $-q_{bnd}$  and  $q_{bnd}$  uniformly distributed along the edges at  $y = 0$  and  $y = L_y$ , respectively [Fig. 1(c)]. Since a superconducting ring threaded

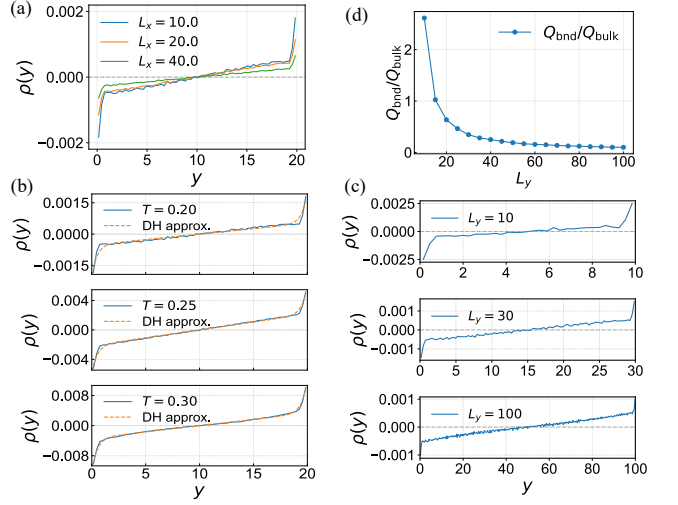


FIG. 2. Induced net charge distribution. (a)–(c) Net charge density  $\rho(y)$  for different values of  $L_x$ , temperature  $T$ , and  $L_y$ , respectively. Other parameters are: (a)  $T = 0.2$ ,  $L_y = 20$ ; (b)  $L_x = 10$ ,  $L_y = 20$ ; (c)  $T = 0.2$ ,  $L_x = 10$ . The dashed lines (b) show  $\rho(y)$  obtained from the DH approximation, Eq. 12. (d) Ratio  $Q_{bnd}/Q_{bulk}$  as a function of  $L_y$ , with  $L_x = 10$  and  $T = 0.2$ .

by  $\Phi = n\Phi_0$  can be absorbed into as a phase winding around the hole of the cylinder, we redefine the boundary charge as  $q_{bnd} = \frac{\Phi}{\Phi_0} - n$ , where  $n$  is chosen such that  $\left| \frac{\Phi}{\Phi_0} - n \right| < \frac{1}{2}$ .

Remarkably, when  $\Phi \neq n\Phi_0$ , the boundary charge  $q_{bnd}$  is finite and fractional. The opposite boundary charge at two edges generates electric fields in the bulk, which in turn induce net positive and negative charge accumulation near the two boundaries, as we would show later. The corresponding dual picture is that the magnetic flux generates a supercurrent that produces Lorentz forces, thereby driving vortex dynamics, as illustrated in Fig. 1(a).

By replacing the field-dependent term in Eq. (7) with the boundary charge term, we find that the dual description of the LP effect near the BKT transition is given by

$$\tilde{S}_{LP} = \beta \int d^2 \mathbf{r} \{ \mathcal{A} |\rho_v| + ia_0(\rho_v + \rho_v^{(A)}) + \frac{|\nabla a_0|^2}{8\pi^2 J} \}. \quad (11)$$

The action  $\tilde{S}_{LP}$  describes a Coulomb gas problem with an additional boundary charge  $\rho_v^{(A)}$ . Compared with previous formulations [24, 26], the present theory explicitly incorporates the external flux in a cylinder/ring geometry, whose effects are the focus of this work.

*Monte Carlo simulation.*— The neutral Coulomb gas model in Eq. (8) is a minimal model for BKT physics and has been studied, primarily using Monte Carlo simulations [27–29]. The key new ingredient in our problem is the presence of opposite boundary charges at the bottom and top edges ( $y = 0, L_y$ ), which effectively gener-

ate external electric fields in the bulk. To screen these boundary charges and reduce the resulting electric fields, charge dipoles are induced in the bulk (see Fig. 1(c)). As a consequence of this screening, positive (negative) charges are attracted toward the edge carrying negative (positive) boundary charge. We therefore perform Monte Carlo simulations to study the bulk net charge distribution  $\rho(y)$  induced by the boundary charges, where  $\rho(y) = \rho_+(y) - \rho_-(y)$  denotes the difference between positive and negative charge densities. The charge distribution is uniform along the  $x$  direction. Details of the Monte Carlo method and model parameters are provided in the SM [25]. For our chosen parameters, the corresponding BKT transition temperature is  $T_{BKT} \approx 0.18$ .

The results are summarized in Fig. 2. Without loss of generality, we set  $q_{bnd} = -0.5$  at  $y = 0$  and  $q_{bnd} = 0.5$  at  $y = L_y$  in the simulations. Figure 2(a) shows the  $L_x$  dependence of the charge distribution  $\rho(y)$  at  $T = 0.2$  and  $L_y = 20$ . Note that the length unit in our simulations is roughly the scale (or a few times) of the superconducting coherence length  $\xi$ . We find that  $\rho(y)$  decays nearly exponentially away from the boundaries due to the presence of boundary charges. As  $L_x$  increases, the boundary charge density is reduced [see Eq. (10)], leading to a suppression of  $\rho(y)$ . Figure 2(b) shows the temperature dependence of  $\rho(y)$ . As expected,  $\rho(y)$  increases rapidly at higher temperatures due to thermally excited positive and negative charge pairs. Clearly, for all parameters considered, the charge distribution satisfies  $\rho(y) = -\rho(-y)$ , consistent with overall charge neutrality.

The charge density profile  $\rho(y)$  can be obtained analytically in the regime where the charge density is sufficiently high to be treated as a continuum with Debye–Hückel (DH) approximation [30]. In this limit, by solving the Poisson equation with boundary charge densities  $\pm\sigma$  imposed at  $y = 0, L_y$  [for details, see SM Sec. III], we obtain

$$\rho(y) \approx -a \frac{\sinh[\kappa(y - L_y/2)]}{\cosh(\kappa L_y/2)} + b y, \quad (12)$$

where  $a \propto \sigma$ ,  $b = \frac{\kappa^2 E_0}{2\pi}$ , and  $\kappa$  is the inverse Debye screening length. The first term originates from the exponentially decaying electric fields near the boundaries, while the second term, linear in  $y$ , arises from a uniform bulk electric field  $E_0$ . The analytical profile in Eq. (12) agrees well with the numerical results [see Fig. 2(b)].

From the above analysis, we identify the bulk region as the region where  $\rho(y)$  varies linearly with  $y$ , while the boundary region is defined as the region within a distance  $\kappa^{-1} \sim 2$  from the edges. As  $L_y$  increases, the bulk region grows monotonically [see Fig. 2(c)]. To compare the charge contributions from the bulk and boundary regions, we define the boundary-induced charge  $Q_{bnd} = \int_0^{\kappa^{-1}} dy \rho(y)$  and the bulk-induced charge  $Q_{bulk} = \int_{\kappa^{-1}}^{L_y/2} dy \rho(y)$ . The ratio  $Q_{bnd}/Q_{bulk}$  as a function of  $L_y$  is shown in Fig. 2(d). We find that the bulk and boundary charges become comparable at  $L_y \sim 20$

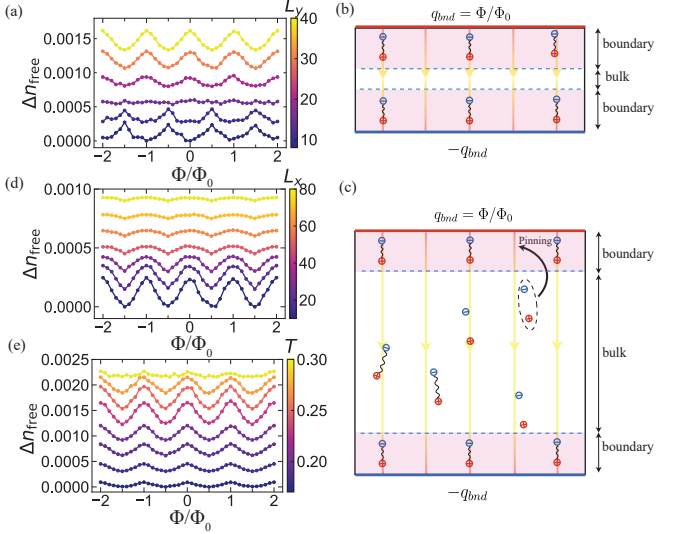


FIG. 3. (a), (d), (e) Oscillations of the free charge density  $\Delta n_{\text{free}}$  as a function of flux  $\Phi/\Phi_0$  for different values of  $L_y$ ,  $L_x$ , and  $T$ , respectively. Parameters are: (a)  $L_x = 10$ ,  $T = 0.2$ ; (d)  $L_y = 30$ ,  $T = 0.2$ ; (e)  $L_x = 10, L_y = 40$ . (b),(c) Schematic illustrations of vortex dynamics involved in screening the boundary charges in the small- $L_y$  and large- $L_y$  limits, respectively. The boundary charges on the two edges are labeled as  $q_{\text{bnd}} = \pm \frac{\Phi}{\Phi_0}$ . Electric field lines generated by the boundary charges are illustrated, with stronger fields near the boundaries (red) and a nearly uniform weak field in the bulk (yellow). As highlighted in (c), the boundary charges tend to attract and pin vortex–antivortex pairs at the boundaries.

for our simulation parameters.

*Half-quantum flux shift in LP oscillations.*— As pointed out above, the boundary charge  $q_{\text{bnd}}$  varies periodically with period  $\Phi_0$ . Consequently, the bulk charge distribution is also expected to exhibit periodic dependence on the magnetic flux. We therefore investigate how the free charge density  $n_{\text{free}}$  varies with the magnetic flux  $\Phi$  in a 2D superconducting ring. We focus on the free charge density because, near the BKT transition, the resistance is dominated by free (i.e., unbound) vortices. As a result, the dependence of  $n_{\text{free}}$  on  $\Phi$  directly corresponds to the LP oscillations of 2D superconductors near the BKT transition. In the Monte Carlo simulations, a charge located at  $\mathbf{r}_i$  is defined as free if the nearest charge of opposite sign at  $\mathbf{r}_j$  satisfies  $|\mathbf{r}_i - \mathbf{r}_j| > r_{\text{free}}$ , where  $r_{\text{free}}$  is the cutoff distance beyond which opposite charges are regarded as unbound. Below, we set  $r_{\text{free}} = 0.7$ , for which the LP oscillations remain clearly visible. Note that varying  $r_{\text{free}}$  mainly affects the amplitude of the LP oscillations (see SM [25]), while the key trends regarding the LP discussed below remain unchanged. The free-vortex density is then defined as  $n_{\text{free}} = \frac{\langle N_{\text{free}} \rangle}{L_x L_y}$ , where  $\langle N_{\text{free}} \rangle$  is the number of free vortices averaged over Monte Carlo measurements. Since the resistance is proportional to  $n_{\text{free}}$ , peaks in the curves at integer (half-integer) flux quanta correspond to the unconventional  $\pi$ -ring (conven-

tional 0-ring) behavior in the LP effect.

Figure 3(a) shows  $\Delta n_{\text{free}}$  as a function of  $\Phi/\Phi_0$  for different values of  $L_y$ , exhibiting the expected oscillations with period  $\Phi_0$ . Here,  $\Delta n_{\text{free}}$  is obtained by subtracting the flux-independent background from  $n_{\text{free}}$  to highlight the oscillatory component. Remarkably, there is an crossover from a 0-ring to a  $\pi$ -ring as  $L_y$  is varied, which occurs around  $Q_{\text{bnd}}/Q_{\text{bulk}} \sim 1$  shown in Fig. 2(d). We now provide an intuitive explanation of the underlying mechanism. As illustrated in Fig. 3(b) and (c), the boundary charge affects the free-vortex density through two competing mechanisms: (i) it generates an electric field that effectively weakens the vortex–antivortex binding energy, thereby promoting the proliferation of free vortices; (ii) it attracts vortex–antivortex pairs from the bulk and pins them at the boundary to screen the electric field. As the boundary charge increases, the first mechanism tends to increase the number of free vortices, whereas the second mechanism tends to suppress it. When  $L_y$  is small so that the boundary regions dominate the system (see Fig. 3(b)), the electric-field effect is dominant. In this regime, free vortices are mainly generated by the boundary electric field, leading to peaks around half-integer flux. In contrast, for larger  $L_y$  [Fig. 3(c)], most free vortices originate from the bulk region, and the dominant effect of the boundary charge is the pinning of vortex pairs at the boundaries. After screening, the electric field in the bulk is much weaker than near the edges. As a result, increasing the boundary charge reduces the number of free vortices, producing peaks at integer flux and yielding the  $\pi$ -ring behavior observed at larger  $L_y$  in Fig. 3(a).

Finally, we examine the dependence of the LP oscillations on the ring perimeter  $L_x$  and temperature  $T$  [see Fig. 3(d) and (e)]. We find that the  $\pi$ -ring behavior driven by the BKT transition is highly robust and persists over a wide range of parameters. In particular, the  $\pi$ -ring survives even for large aspect ratios  $L_x/L_y \gg 1$ , although increasing  $L_x$  is expected to reduce the absolute oscillation amplitude.

*Discussion.*— In summary, we have established a theoretical framework for the LP effect induced by vortices near the BKT transition in 2D superconductors. In particular, we have shown that half-quantum flux shifts can emerge in this regime. We anticipate that our theory can be experimentally tested in a variety of 2D superconductors by investigating the interplay between LP oscillations and BKT physics.

How the LP oscillations evolve from the temperature regime near  $T_{\text{BKT}}$  to that close to the mean-field transition temperature  $T_c$  remains an open issue. Preliminary experimental studies in this direction may provide valuable insights. Finally, since the binding energy of vortex–antivortex pairs is also affected by external supercurrents, understanding how supercurrents modify the LP oscillations discussed in this work constitutes another interesting open question.

*Acknowledgment.*— We are very grateful for the in-

sightful discussions with Bertrand Halperin, Leonid Glazman, and Yasuhiro Tokura. Y.M.X. acknowledges financial support from the RIKEN Special Postdoctoral Researcher (SPDR) Program. N.N. was supported by JSPS KAKENHI Grant No.24H00197, 24H02231, and 24K00583. N.N. was also supported by the RIKEN TRIP initiative.

- [1] B. S. Deaver and W. M. Fairbank, *Phys. Rev. Lett.* **7**, 43 (1961).
- [2] R. Doll and M. N  bauer, *Phys. Rev. Lett.* **7**, 51 (1961).
- [3] W. A. Little and R. D. Parks, *Phys. Rev. Lett.* **9**, 9 (1962).
- [4] R. D. Parks and W. A. Little, *Phys. Rev.* **133**, A97 (1964).
- [5] M. Tinkham, *Introduction to superconductivity* (Courier Corporation, 2004).
- [6] G. Grosso and G. P. Parravicini, *Solid state physics* (Academic press, 2013).
- [7] C. C. Tsuei and J. R. Kirtley, *Rev. Mod. Phys.* **72**, 969 (2000).
- [8] M. Sigrist, *AIP Conference Proceedings* **789**, 165 (2005).
- [9] V. B. Geshkenbein, A. I. Larkin, and A. Barone, *Phys. Rev. B* **36**, 235 (1987).
- [10] S. B. Chung, H. Bluhm, and E.-A. Kim, *Phys. Rev. Lett.* **99**, 197002 (2007).
- [11] V. Vakaryuk and A. J. Leggett, *Phys. Rev. Lett.* **103**, 057003 (2009).
- [12] M. M. Salomaa and G. E. Volovik, *Phys. Rev. Lett.* **55**, 1184 (1985).
- [13] Y. Li, X. Xu, M.-H. Lee, M.-W. Chu, and C. L. Chien, *Science* **366**, 238 (2019).
- [14] X. Xu, Y. Li, and C. L. Chien, *Phys. Rev. Lett.* **124**, 167001 (2020).
- [15] Z. Wan, G. Qiu, H. Ren, Q. Qian, Y. Li, D. Xu, J. Zhou, J. Zhou, B. Zhou, L. Wang, T.-H. Yang, Z. Sofer, Y. Huang, K. L. Wang, and X. Duan, *Nature* **632**, 69 (2024).
- [16] A. Almoalem, I. Feldman, I. Mangel, M. Shlafman, Y. E. Yaish, M. H. Fischer, M. Moshe, J. Ruhman, and A. Kanigel, *Nature Communications* **15**, 4623 (2024).
- [17] M. Tokuda, F. Matsumoto, N. Maeda, T. Higashihara, M. Nakao, M. Watanabe, S. Lee, R. Nakamura, M. Maeda, N. Jiang, D. Yue, H. Narita, K. Aoyama, T. Mizushima, J. ichiro Ohe, T. Ono, X. Jin, K. Kobayashi, and Y. Niimi, *Science Advances* **11**, eadw6625 (2025).
- [18] S. Wang, I. Maccari, X. Feng, Z.-N. Wu, J.-P. Peng, K. Tuen Law, Y. X. Zhao, A. Szabo, A. Schnyder, N. Kang, X.-S. Wu, J. Liu, X. Fu, M. H. Fischer, M. Sigrist, D. Yu, and B.-C. Lin, *arXiv e-prints* , arXiv:2512.10010 (2025).
- [19] E. Zhang, Y.-M. Xie, S. Liu, Y. Fang, J. Zhang, Y.-C. Zou, Y. Zhang, Z. Jia, J. Chen, Q. Ma, W. Zhao, K. P. Loh, F. Huang, and F. Xiu, manuscript submitted.
- [20] K. Aoyama, *Phys. Rev. B* **106**, L060502 (2022).
- [21] M. H. Fischer, P. A. Lee, and J. Ruhman, *Phys. Rev. B* **108**, L180505 (2023).
- [22] C. Hua, E. Dumitrescu, and G. B. Hal  sz, *Phys. Rev. B* **107**, 214503 (2023).
- [23] J. Zhang and Y. Li, *arXiv e-prints* , arXiv:2509.24581 (2025).
- [24] N. Nagaosa, *Quantum field theory in condensed matter physics* (Springer Science & Business Media, 2013).

- [25] See the Supplementary Material for (i) field theory details for Little-Parks oscillations near BKT transitions, (ii) Monte Carlo Simulation Method, (iii) induced charge density distribution under the DH approximation.
- [26] M. P. A. Fisher and D. H. Lee, *Phys. Rev. B* **39**, 2756 (1989).
- [27] J. M. Kosterlitz and D. J. Thouless, *Journal of Physics C: Solid State Physics* **6**, 1181 (1973).
- [28] J.-R. Lee and S. Teitel, *Phys. Rev. B* **46**, 3247 (1992).
- [29] J. Lidmar and M. Wallin, *Phys. Rev. B* **55**, 522 (1997).
- [30] D. A. McQuarrie, *Statistical Mechanics* (Harper & Row, New York, 1976).

# Supplementary Material for “ Theory of Little–Parks oscillations by vortices in two-dimensional superconductors ”

Ying-Ming Xie<sup>1</sup> and Nato Nagaosa<sup>1,2</sup>

<sup>1</sup> RIKEN Center for Emergent Matter Science (CEMS), Wako, Saitama 351-0198, Japan

<sup>2</sup> Fundamental Quantum Science Program (FQSP), TRIP Headquarters, RIKEN, Wako 351-0198, Japan

## CONTENTS

I. Field theory details for Little-Parks oscillations near BKT transitions	1
A. Field theory near the BKT transition for 2D superconductors	1
B. Map to a Coulomb gas problem	2
C. Dual-field theory description of the Little-Parks effect near BKT transition	3
II. Monte Carlo Simulation Method	4
A. Monte Carlo simulation for 2D neutral Coulomb gas	4
B. Boundary potential from uniform line charges	5
III. Induced charge density distribution under the DH approximation	6

## I. FIELD THEORY DETAILS FOR LITTLE-PARKS OSSILATIONS NEAR BKT TRANSITIONS

### A. Field theory near the BKT transition for 2D superconductors

The action is given by

$$S = \int d^3\tilde{x} \frac{J}{2} (\partial_\mu \theta + 2eA_\mu)^2. \quad (\text{S1})$$

All notation used in the Supplementary Material follows the definitions in the main text. To proceed, we decompose the phase field into a smooth part and a vortex-core contribution,

$$\theta = \theta_0 + \theta_v.$$

Applying a Hubbard–Stratonovich transformation to decouple the quadratic term yields

$$\exp\left[-\int d^3\tilde{x} \frac{J}{2} (\partial_\mu \theta + 2eA_\mu)^2\right] \propto \int DJ_\mu \exp\left[-\int d^3\tilde{x} \left(\frac{J_\mu^2}{2J} + iJ_\mu(\partial_\mu \theta_0 + \partial_\mu \theta_v + 2eA_\mu)\right)\right]. \quad (\text{S2})$$

The partition function can therefore be written as

$$Z = \int D\theta_0 D\theta_v DJ_\mu \exp\left[-\int d^3\tilde{x} \left(\frac{J_\mu^2}{2J} + iJ_\mu(\partial_\mu \theta_0 + \partial_\mu \theta_v + 2eA_\mu)\right)\right]. \quad (\text{S3})$$

We now isolate the contribution involving the smooth phase field  $\theta_0$ ,

$$S[\theta_0] = \int d^3\tilde{x} iJ_\mu \partial_\mu \theta_0 = - \int d^3\tilde{x} i(\partial_\mu J_\mu) \theta_0, \quad (\text{S4})$$

where the second equality follows from integration by parts, assuming vanishing boundary terms. Performing the functional integral over  $\theta_0$  enforces the conservation of the auxiliary current,

$$\int D\theta_0 e^{-S[\theta_0]} = \int D\theta_0 \exp\left(\int d^3\tilde{x} i(\partial_\mu J_\mu) \theta_0\right) \propto \delta[\partial_\mu J_\mu]. \quad (\text{S5})$$

After integrating out  $\theta_0$ , the partition function reduces to

$$Z = \int D\theta_v DJ_\mu \delta[\partial_\mu J_\mu] \exp\left[-\int d^3\tilde{x} \left(\frac{J_\mu^2}{2J} + iJ_\mu(\partial_\mu \theta_v + 2eA_\mu)\right)\right]. \quad (\text{S6})$$

The conservation of supercurrent  $\partial_\mu J_\mu = 0$ , resulting in

$$J_\mu = \frac{1}{2\pi} \epsilon_{\mu\nu\lambda} \partial_\nu a_\lambda = \frac{1}{2\pi} \nabla_{3D} \times a_{3D}. \quad (\text{S7})$$

$$\int d^3 \tilde{x} i J_\mu(x) \partial_\mu \theta_v = \int d^3 \tilde{x} i \frac{1}{2\pi} \epsilon_{\mu\nu\lambda} \partial_\nu a_\lambda \partial_\mu \theta_v = \int d^3 \tilde{x} i \frac{1}{2\pi} \epsilon_{\nu\mu\lambda} a_\lambda \partial_\nu \partial_\mu \theta_v = \int d^3 \tilde{x} i a_\lambda j_\lambda \quad (\text{S8})$$

$$2e \int d^3 \tilde{x} \frac{i}{2\pi} \epsilon_{\mu\nu\lambda} \partial_\nu a_\lambda A_\mu = \frac{e}{\pi} \int d^3 \tilde{x} i a_\lambda B_\lambda \quad (\text{S9})$$

The resulting effective action is

$$\tilde{S}' = A \sum_i \int ds_i + \int d^3 x \frac{(\nabla_{3D} \times a_{3D})^2}{8\pi^2 J} + i \int d^3 x a_{3D} \cdot \left( j_{3D} + \frac{e}{\pi} B_{3D} \right). \quad (\text{S10})$$

The first term on the right-hand side represents the energy cost associated with vortex cores, with an action  $A$  per unit length multiplied by the length of the world line  $\int ds_i$  of the  $i$ th vortex.

In the static two-dimensional limit, the imaginary-time integral reduces to  $\int_0^\beta d\tau = \beta$ . Moreover,

$$(\nabla_{3D} \times a_{3D})^2 = F_\mu F_\mu, \quad (\text{S11})$$

where  $F_\mu = \epsilon_{\mu\nu\lambda} \partial_\nu a_\lambda$ . Explicitly, the components are

$$F_0 = \epsilon_{0ij} \partial_i a_j = \partial_x a_y - \partial_y a_x, \quad (\text{S12})$$

$$F_i = \epsilon_{i0j} \partial_0 a_j + \epsilon_{ij0} \partial_j a_0 = -\epsilon_{ij} \partial_0 a_j + \epsilon_{ij} \partial_j a_0. \quad (\text{S13})$$

The external magnetic field is given by  $B_{3D} = B_0 = \epsilon_{0\nu\mu} \partial_\nu A_\mu = \nabla_{2D} \times \mathbf{A} = B_z \hat{\mathbf{z}}$ .

In the static limit, we may set  $a_i = 0$  since the spatial components do not couple to the vortex density, and  $\partial_0 a_i = 0$ . Consequently, the theory reduces to the mapping

$$a_{3D} \mapsto a_0(\mathbf{r}), \quad j_\mu \mapsto j_0 = \rho_v(\mathbf{r}), \quad B_{3D} \mapsto B_0 = B_z. \quad (\text{S14})$$

The effective action then becomes

$$\tilde{S}' = \beta \int d^2 \mathbf{r} \left\{ A |\rho_v(\mathbf{r})| + i a_0(\mathbf{r}) \left( \rho_v(\mathbf{r}) + \frac{e}{\pi} B_z \right) + \frac{|\nabla a_0(\mathbf{r})|^2}{8\pi^2 J} \right\}. \quad (\text{S15})$$

This action describes a two-dimensional Coulomb gas.

## B. Map to a Coulomb gas problem

Let us take the vortex charge density to be

$$\rho_v = \sum_i q_i \delta(\mathbf{r} - \mathbf{X}_i). \quad (\text{S16})$$

Here  $q_i = \pm 1$  corresponds to a vortex or an antivortex, and  $\mathbf{X}_i$  denotes the position of the  $i$ -th vortex core. We now integrate out the scalar field  $a_0(\mathbf{r})$  in the zero-field limit ( $B_z = 0$ ).

The action is

$$\tilde{S}'[a_0, \rho_v] = \int d^2 r \left[ \frac{1}{8\pi^2 J} (\nabla a_0)^2 + i a_0(\mathbf{r}) \rho_v(\mathbf{r}) \right] \quad (\text{S17})$$

$$= \int d^2 r \left[ -\frac{1}{8\pi^2 J} a_0 \nabla^2 a_0 + i a_0(\mathbf{r}) \rho_v(\mathbf{r}) \right], \quad (\text{S18})$$

where the second line follows from integration by parts.

Using the standard Gaussian integral formula

$$\int D\phi e^{-\frac{1}{2}(\phi, K\phi)+(J, \phi)} \propto \exp\left[\frac{1}{2}(J, K^{-1}J)\right],$$

we obtain

$$Z \propto \exp\left[-\frac{1}{2}(\rho_v, K^{-1}\rho_v)\right] = \exp\left[-\frac{1}{2} \int d^2r d^2r' \rho_v(\mathbf{r}) V(\mathbf{r} - \mathbf{r}') \rho_v(\mathbf{r}')\right]. \quad (\text{S19})$$

Here the interaction kernel  $V(\mathbf{r})$  is defined through the relation  $KV(\mathbf{r}) = \delta(\mathbf{r})$ , which implies

$$\nabla^2 V(\mathbf{r}) = -4\pi^2 J \delta(\mathbf{r}). \quad (\text{S20})$$

In Fourier space, this yields  $V(\mathbf{k}) = 4\pi^2 J/k^2$ . We also make use of the identity

$$\int \frac{d^2k}{(2\pi)^2} \frac{e^{i\mathbf{k}\cdot\mathbf{r}}}{k^2} = -\frac{1}{2\pi} \ln \frac{r}{r_c}, \quad (\text{S21})$$

where  $r_c$  is a short-distance cutoff.

The effective action therefore becomes

$$\begin{aligned} \tilde{S}_{\text{eff}} &= \frac{1}{2} \int d^2r d^2r' \rho_v(\mathbf{r}) V(\mathbf{r} - \mathbf{r}') \rho_v(\mathbf{r}') \\ &= \frac{1}{2} \sum_{i \neq j} q_i q_j V(\mathbf{X}_{ij}) + E_c \sum_i q_i^2, \end{aligned} \quad (\text{S22})$$

where  $\mathbf{X}_{ij} = \mathbf{X}_i - \mathbf{X}_j$ , and the vortex core energy is given by  $E_c = \frac{1}{2}V(0)$ . The interaction potential between vortices is

$$V(\mathbf{X}_{ij}) = -2\pi J \ln \frac{|\mathbf{X}_{ij}|}{r_c}. \quad (\text{S23})$$

### C. Dual-field theory description of the Little-Parks effect near BKT transition

We consider a superconducting cylinder of radius  $R$ , threaded by a magnetic flux  $\Phi$  through its center. Inside the sample, the magnetic field satisfies  $B_z = 0$ , while the vector potential  $\mathbf{A}$  remains nonzero, corresponding to an Aharonov–Bohm configuration. The central question is how the vector potential  $\mathbf{A}$  affects the Kosterlitz–Thouless transition.

From the dual action, the coupling to the external field is given by

$$\int d^3x \frac{ie}{\pi} \partial_\nu a_\lambda A_\mu = \frac{ie}{\pi} \int d^3x (\nabla_{3D} \times \mathbf{a}_{3D}) \cdot \mathbf{A}_{3D}. \quad (\text{S24})$$

Using the vector identity

$$\nabla \cdot (\mathbf{c} \times \mathbf{d}) = \mathbf{d} \cdot (\nabla \times \mathbf{c}) - \mathbf{c} \cdot (\nabla \times \mathbf{d}), \quad (\text{S25})$$

and replacing  $\mathbf{c} = \mathbf{a}_{3D}$ ,  $\mathbf{d} = \mathbf{A}_{3D}$ , together with the condition  $\nabla_{3D} \times \mathbf{A}_{3D} = 0$  inside the sample region, we obtain in the static limit

$$\begin{aligned} \int d^3x \frac{ie}{\pi} \partial_\nu a_\lambda A_\mu &= \frac{ie}{\pi} \int d^3x \nabla \cdot (\mathbf{a}_{3D} \times \mathbf{A}_{3D}) \\ &= \frac{ie\beta}{\pi} \int_{\partial V} d^2r \cdot (\mathbf{a}_{3D} \times \mathbf{A}_{3D}). \end{aligned} \quad (\text{S26})$$

The boundaries of the cylinder are located at  $y = 0$  and  $y = L$ , and

$$\mathbf{a}_{3D} \times \mathbf{A}_{3D} = (a_x A_y - a_y A_x, a_y A_0 - a_0 A_y, a_0 A_x - a_x A_0). \quad (\text{S27})$$

In the static limit  $A_0 = 0$ , this reduces to

$$\int d^3x \frac{ie}{\pi} \partial_\nu a_\lambda A_\mu = \frac{ie\beta}{\pi} \int d^2r a_0 A_x [\delta(y - L) - \delta(y)]. \quad (\text{S28})$$

Upon unwrapping the cylindrical geometry into Cartesian coordinates  $(x, y)$ , the vector potential becomes  $A_x = \Phi/(2\pi R)$ . The effective field-theoretic description of the Little–Parks experiment near the BKT transition is then given by

$$S_{BKT} = \beta \int d^2r \left[ ia_0(\mathbf{r}) (\rho_v(\mathbf{r}) + \rho_v^{(A)}(\mathbf{r})) + \frac{|\nabla a_0(\mathbf{r})|^2}{8\pi^2 J} \right]. \quad (\text{S29})$$

Here the boundary-induced vortex charge density is

$$\rho_v^{(A)}(\mathbf{r}) = \frac{e\Phi}{2\pi^2 R} [\delta(y - L) - \delta(y)]. \quad (\text{S30})$$

We have neglected the vortex core energy contribution (the first term in Eq. (S10)), since it merely shifts the overall normalization of the partition function.

Because  $\hbar = 1$ , the superconducting flux quantum is  $\Phi_0 = \pi/e$ . For flux values  $\Phi = n\Phi_0$ , the vector potential can be absorbed as a large vortex trapped inside the cylinder. We therefore redefine the boundary vortex charge density as

$$\rho_v^{(A)} = \frac{q_{bnd}}{L_x} [\delta(y - L) - \delta(y)], \quad (\text{S31})$$

where

$$q_{bnd} = \left( \frac{\Phi}{\Phi_0} - n \right), \quad (\text{S32})$$

and  $n$  is an integer chosen such that  $|\Phi/\Phi_0 - n| < \frac{1}{2}$ .

## II. MONTE CARLO SIMULATION METHOD

### A. Monte Carlo simulation for 2D neutral Coulomb gas

We simulate a two-dimensional Coulomb gas representing vortex–antivortex excitations of the XY model near the Kosterlitz–Thouless (KT) transition. Each configuration consists of integer charges  $q_i = \pm 1$  interacting via a logarithmic potential

$$E = - \sum_{i < j} q_i q_j \ln \left( \frac{\mathbf{X}_{ij}}{r_c} \right),$$

with a short-range cutoff  $r_{\min}$ . The Coulomb gas is charge neutral with  $\sum_i q_i = 0$ . The system is defined on a square of size  $L \times L$ .

Monte Carlo sampling is performed using a Metropolis algorithm that combines (i) displacement moves of existing vortices, (ii) creation of vortex–antivortex pairs, and (iii) annihilation of existing pairs. Each move is accepted with probability  $\min[1, e^{-\beta \Delta E}]$ , with energy differences  $\Delta E$  computed efficiently using Numba-accelerated routines. The creation and destruction moves include the appropriate phase-space and chemical potential factors to satisfy detailed balance. We followed the Monte Carlo simulation method in Ref. [29]. But for completeness, let us explain the Monte Carlo updates in more detail below.

We simulate a two-dimensional Coulomb gas in the grand-canonical ensemble at inverse temperature  $\beta$  and chemical potential  $\mu$  per particle. A configuration  $C$  consists of  $N$  charges  $\{(q_i, \mathbf{r}_i)\}$  with  $q_i = \pm 1$  and statistical weight

$$\mathcal{P}(C) \propto \exp[-\beta(E(C) - \mu N)]. \quad (\text{S33})$$

Charge neutrality is enforced by allowing only the creation and destruction of neutral  $(+, -)$  pairs. For pair creation, starting from a configuration  $C$  with  $N = 2n_{\text{old}}$  particles, a trial move  $C \rightarrow C'$  is proposed as follows: a  $+1$  charge is inserted uniformly over the system area  $V = L_x L_y$ , followed by the insertion of a  $-1$  charge uniformly within a disk

TABLE S1. Key parameters used in the Monte Carlo simulation of the 2D neutral Coulomb gas.

Parameter	Symbol / Value	Description
Chemical potential	$\mu = -0.80$	Controls vortex pair density
Core cutoff	$r_{\min} = 0.35$	Hard-core exclusion radius
Interaction scale	$r_c = 0.94$	Reference distance in $\log(r/r_c)$ interaction
Maximum separation	$d = 1$	the maximum separation for a local pair
Thermalization	$N_{\text{therm}} = 2.0 \times 10^4$	Number of equilibration sweeps
Measurement	$N_{\text{meas}} = 10.0 \times 10^4$	Number of measurement sweeps
Measurement interval	$N_{\text{skip}} = 20$	Sweeps between successive measurements

of radius  $d$ . The corresponding proposal area is  $\Omega \equiv V_b = \pi d^2$ . The move is rejected immediately if any hard-core constraint is violated (e.g., if interparticle distances are smaller than  $r_{\min}$ ). The trial probability density for pair creation is therefore  $t_{\text{cre}}(C \rightarrow C') = \frac{1}{V\Omega}$ . For the reverse move  $C' \rightarrow C$ , the system contains  $n_{\text{new}} = \frac{N+2}{2} = n_{\text{old}} + 1$  neutral pairs. One pair is chosen uniformly at random and removed, yielding the trial probability  $t_{\text{des}}(C' \rightarrow C) = \frac{1}{n_{\text{new}}}$ . Let  $\Delta E = E(C') - E(C)$  denote the total energy change associated with inserting the proposed pair, including all interaction and boundary contributions. Detailed balance requires

$$\mathcal{P}(C) t(C \rightarrow C') \tilde{a}(C \rightarrow C') = \mathcal{P}(C') t(C' \rightarrow C) \tilde{a}(C' \rightarrow C), \quad (\text{S34})$$

where  $\tilde{a}$  denotes the acceptance probability. Using the Metropolis choice  $a = \min(1, R)$ , the acceptance ratio for pair creation is  $R_{\text{cre}} = \frac{V\Omega}{n_{\text{old}}+1} \exp[-\beta(\Delta E - 2\mu)]$ . The creation move is therefore accepted with probability  $a_{\text{cre}} = \min\left[1, \frac{V\Omega}{n_{\text{old}}+1} \exp(-\beta(\Delta E - 2\mu))\right]$ . The corresponding destruction move uses the inverse ratio,  $a_{\text{des}} = \min(1, R_{\text{cre}}^{-1})$ . After a thermalization period of approximately  $2 \times 10^4$  sweeps, measurements are collected every few sweeps over about  $10 \times 10^4$  updates. For convenience, the key Monte Carlo parameters are summarized in Table S1. The determination of  $T_{\text{BKT}}$  and the effects of various  $r_{\text{free}}$  are discussed in Fig. S1.

## B. Boundary potential from uniform line charges

We consider a two-dimensional Coulomb gas confined between two open boundaries at  $y = 0$  and  $y = L_y$ , with periodic boundary conditions along  $x$ . Each boundary carries a uniform line charge of opposite sign,  $-\lambda$  at  $y = 0$  and  $+\lambda$  at  $y = L_y$ , producing a one-body potential acting on mobile charges in the interior.

The electrostatic potential at position  $(x, y)$  due to a uniform line charge with density  $\lambda$  along  $x' \in [0, L_x]$  at height  $y_0$  is

$$V_{\text{line}}(x, y) = -\lambda \int_0^{L_x} \ln \sqrt{(x - x')^2 + (y - y_0)^2} dx'. \quad (\text{S35})$$

Since the line is translationally invariant in  $x$ , the result depends only on the vertical separation  $a = |y - y_0|$ . Evaluating the integral gives

$$\Gamma(a, L_x) \equiv \int_0^{L_x} \ln \sqrt{u^2 + a^2} du = \frac{1}{2} L_x \ln(L_x^2 + a^2) + a \arctan \frac{L_x}{a} - L_x. \quad (\text{S36})$$

Up to an additive constant (which cancels in  $\Delta E$ ), the potential of a single uniform line is therefore  $V_{\text{line}}(y) = -\lambda \Gamma(|y - y_0|, L_x)$ .

Superposing the two boundary contributions at  $y = 0$  and  $y = L_y$  gives the total one-body potential

$$V_{\text{bnd}}(y) = -\lambda \Gamma(L_y - y, L_x) + \lambda \Gamma(y, L_x). \quad (\text{S37})$$

Introducing the total boundary charge per line,  $q_{\text{bnd}} = \lambda L_x$ , one obtains the exact form

$$V_{\text{bnd}}(y) = -\frac{q_{\text{bnd}}}{L_x} \left[ \Gamma(L_y - y, L_x) - \Gamma(y, L_x) \right]. \quad (\text{S38})$$

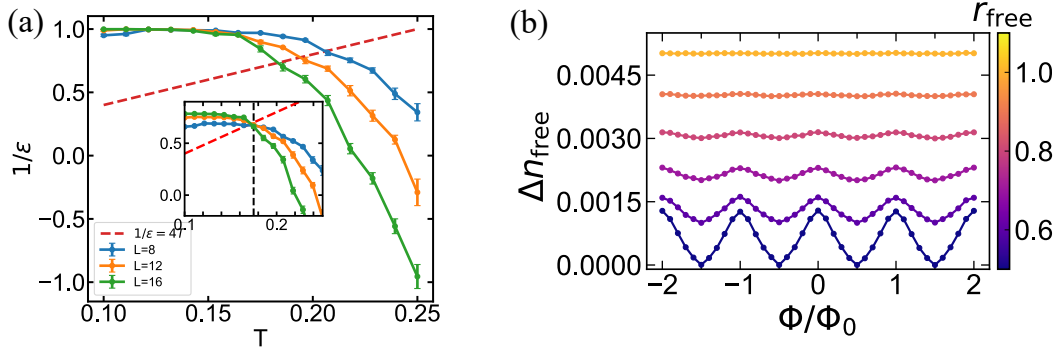


FIG. S1. (a) The inverse dielectric constant as a function of the system size  $L \times L$ . Here,  $\epsilon^{-1} = 1 - \frac{\pi}{L^2 T} \langle P_x^2 + P_y^2 \rangle$ , where  $\mathbf{P} = \sum_i q_i(\mathbf{r}_i - L/2)$  is the total dipole moment. The inset shows the data after applying a finite-size correction,  $\frac{1}{\epsilon(T, L)} = A(T) \left[ 1 + \frac{1}{2 \ln L + C} \right]$ , following Ref. [29]. The curves intersect at  $T_{\text{BKT}} \simeq 0.18$ , consistent with the Kosterlitz–Thouless critical behavior. (b) The change in the free vortex density  $\Delta n_{\text{free}}$  as a function of  $\Phi/\Phi_0$  for different values of  $r_{\text{free}}$ . The amplitude of the periodic oscillations gradually decreases as  $r_{\text{free}}$  increases. However, the positions of the peaks and dips are insensitive to  $r_{\text{free}}$ , and the  $\pi$ -ring behavior remains robust against variations in  $r_{\text{free}}$ .

### III. INDUCED CHARGE DENSITY DISTRIBUTION UNDER THE DH APPROXIMATION

The charge density in the bulk can be expressed as

$$\begin{aligned} \rho(\mathbf{r}) &= n_+ e^{-\beta q_+ \phi(\mathbf{r})} - n_- e^{+\beta q_- \phi(\mathbf{r})} \\ &= -2n_0 \sinh[\beta \phi(\mathbf{r})], \end{aligned} \quad (\text{S39})$$

where  $\phi(\mathbf{r})$  denotes the electrostatic potential field, and we have assumed charge symmetry with  $n_+ = n_- = n_0$  and  $q_+ = -q_- = 1$ .

The electrostatic potential satisfies the two-dimensional Poisson equation,

$$\nabla^2 \phi(\mathbf{r}) = -2\pi\rho(\mathbf{r}). \quad (\text{S40})$$

Substituting the expression for  $\rho(\mathbf{r})$  yields

$$\nabla^2 \phi(\mathbf{r}) = 4\pi n_0 \sinh[\beta \phi(\mathbf{r})]. \quad (\text{S41})$$

In the weak-potential limit ( $\beta\phi \ll 1$ ), we linearize the hyperbolic sine function,  $\sinh(\beta\phi) \simeq \beta\phi$ . This leads to the linearized Debye–Hückel (DH) approximation,

$$\nabla^2 \phi(\mathbf{r}) = \kappa^2 \phi(\mathbf{r}), \quad (\text{S42})$$

where the inverse Debye length is defined as

$$\kappa = \sqrt{\frac{4\pi n_0}{\rho_0}}. \quad (\text{S43})$$

Before solving this differential equation explicitly, we can expect that the solution of this equation near the boundary decays exponentially,  $\phi(r) \sim e^{-r/\lambda_D}$ , with the *Debye screening length*

$$\lambda_D = \frac{1}{\kappa} = \frac{1}{\sqrt{4\pi \beta n_0}}. \quad (\text{S44})$$

Therefore, in the linearized regime, the potential and the induced charge density both decay over the characteristic length scale  $\lambda_D$ . Consequently, the localization length of the boundary-induced charge distribution is governed by the Debye length  $\lambda_D$ . According to Ref. [27],

$$n_0 \approx \frac{1}{\xi_+^2} \quad (\text{S45})$$

where the characteristic length scale controlling the vortex density is  $\xi_+ = \xi_0 \exp\left(\frac{b}{\sqrt{t}}\right)$ , with  $t = \frac{T-T_{\text{BKT}}}{T_{\text{BKT}}}$ . Hence,

$$\lambda_D \propto \xi_+ = \xi_0 \exp[b/\sqrt{t}]. \quad (\text{S46})$$

Let us perform a preliminary estimate of the order of magnitude of the vortex density. In practice,  $b \sim 1$  [27]. Using  $T_{\text{BKT}} = 0.18$ , we estimate  $n_0(T=0.2) \sim 10^{-4}\text{--}10^{-3}$ , which is consistent with the numerical results presented in the main text (see Fig. 3).

Now we solve Eq. (S42) in a more accurate manner. In the cylindrical geometry, the system is periodic along the  $x$ -direction. The equation then simplifies to

$$\frac{\partial^2 \phi}{\partial y^2} = \kappa^2 \phi(y). \quad (\text{S47})$$

According to Gauss's law,  $\hat{\mathbf{n}} \cdot \mathbf{E} = \sigma/\varepsilon$ , where  $\hat{\mathbf{n}}$  is the surface normal vector,  $\sigma$  is the surface charge density, and  $\varepsilon$  is the dielectric permittivity. Since the surface normals and charge densities at  $y=0$  and  $y=L$  are opposite with a boundary charge of  $+\sigma$  and  $-\sigma$  respectively, the boundary conditions are

$$\phi'(0) = \phi'(L) = \frac{\sigma}{\varepsilon}. \quad (\text{S48})$$

We take the ansatz

$$\phi(y) = \phi_{\text{DH}}(y) - E_0 y, \quad (\text{S49})$$

where  $E_0 = \sigma_{\text{net}}/\varepsilon$  characterizes the residual uniform electric field that remains after screening. By solving the differential equation with the above boundary conditions, we obtain

$$\phi(y) = \left( \frac{\sigma}{\varepsilon \kappa} + \frac{E_0}{\kappa} \right) \frac{\sinh[\kappa(y - L/2)]}{\cosh(\kappa L/2)} - E_0 y, \quad (\text{S50})$$

The carrier density is then given by

$$\rho(y) \approx -\frac{\kappa^2}{2\pi} \phi(y) = -a \frac{\sinh[\kappa(y - L/2)]}{\cosh(\kappa L/2)} + b y, \quad (\text{S51})$$

where  $a = \frac{\kappa}{2\pi} \left( \frac{\sigma}{\varepsilon} + E_0 \right)$  and  $b = \frac{\kappa^2 E_0}{2\pi}$ .